Plasma membrane association and resistosome formation of plant helper immune receptors

Zaiqing Wang [1, #], Xiaoxiao Liu [1, #], Jie Yu [1], Shuining Yin [1], Wenjuan Cai [1], Nak Hyun Kim [2], Farid El Kasmi [3], Jeffery L. Dangl [2] and Li Wan [1, *]

[1] National Key Laboratory of Plant Molecular Genetics, CAS Center for Excellence in Molecular Plant Sciences, Institute of Plant Physiology and Ecology, Chinese Academy of Sciences, Shanghai, China.

[2] Department of Biology and Howard Hughes Medical Institute, University of North Carolina at Chapel Hill, Chapel Hill, NC 27599, USA.

[3] Centre for Plant Molecular Biology (ZMBP), University of Tubingen, 72076 Tubingen, Germany.

[#] Z.W., X.L. contributed equally to this work

*Corresponding author: Li Wan

Email: lwan@cemps.ac.cn

Author Contributions: L.W., J.L.D, Z.W., X.L. designed research. Z.W., X.L., J.Y. S.Y., W.C. performed research. Z.W., X.L., L.W., J.L.D, F.E.K., J.Y., N.H.K. analyzed data. L.W. and J.L.D wrote the paper.

Competing Interest Statement: The authors declare no competing interests.

Classification: Plant biology/immunology/biochemistry

Keywords: Plant immunity/NLR immune receptor/helper NLR/cell death

This PDF file includes:

Main Text
Figures 1 to 5
SI Figures 1 to 5

Abstract

Intracellular plant immune receptors, termed NLRs, respond to pathogen effectors delivered into plant cells. Activation of NLRs typically confers strong immunity. Sensor NLRs, involved in effector recognition, are either TIR-NLRs (TNLs) or CC-NLRs (CNLs). Helper NLRs, required for sensor NLR signaling, include CC^R-NLRs (RNLs) and a special class of CNLs known as NRCs. Activated TNLs produce small molecules that induce an association between the EDS1/SAG101 heterodimer and the NRG1s helper RNLs. Auto active NRG1s oligomerize and form calcium signaling channels largely localized at the plasma membrane (PM). The molecular mechanisms of helper NLR PM association and effector induced NRG1 oligomerization remain uncharacterized. We find that both RNLs and NRCs require positively charged residues in the second and fourth helices of their CC^R or CC domain for phospholipid binding and PM association before and after activation, despite conformational changes that accompany activation. We demonstrate that effector activation of TNLs induces NRG1 oligomerization at the PM and the cytoplasmic pool of EDS1/SAG101 is critical for cell death function. EDS1/SAG101 are absent from the oligomerized NRG1 resistosome, suggesting that additional unknown triggers might be required to induce the dissociation of EDS1/SAG101 from the NRG1/EDS1/SAG101 heterotrimer before subsequent NRG1 oligomerization. Our data provide new observations regarding dynamic PM association during helper NLR activation and underpin an updated model for effector induced NRG1 resistosome formation.

Main Text

Introduction

Plants employ both cell surface and intracellular immune receptors to detect pathogens. Cell surface Pattern Recognition Receptors (PRRs) recognize Pathogen-Associated Molecular Patterns (PAMPs) and initiate PAMP-triggered immunity (PTI) (1). Intracellular immune receptors known as Nucleotide-binding Leucine-rich repeat Receptor (NLR) proteins recognize corresponding effectors secreted by pathogens into plant cells and initiate effector-triggered immunity (ETI) (2). Plant NLRs express three main types of N-terminal domains: either a Toll/interleukin-1 receptor (TIR) domain, a coiled-coil (CC) domain, or an RPW8 (Resistance to Powdery Mildew 8)-like CC (CC^R) domain. CC and CC^R domains adopt a conserved

structure fold of 4 helical bundle (4HB) with the CC^R expressing an extra N-terminal region (3). TIR-NLR, CC-NLR and CC^R-NLR are known as TNL, CNL and RNL, respectively (4). TNL and CNL recognize pathogen effectors to trigger cell death and immune responses and are thus termed sensor NLRs. Downstream of sensor NLRs, higher plants also deploy helper NLRs to transduce signals. There are three described classes of helper NLRs. The Activated Disease Resistance 1 (ADR1) family, and the N Required Gene 1 (NRG1) family are highly conserved across the land plant phylogeny (5-7). ADR1s and NRG1s belong to the RNL family and are partially redundant downstream immune mediators of TNLs and some CNLs (8). NRCs are a greatly expanded helper NLR class in several plant families, including the Solanaceae (9). NRCs contain canonical CC domains at their N-termini. In *Nicotiana benthmiana* (*Nb*), three NRCs function redundantly downstream of diverse sensor CNLs to regulate cell death and immune responses (10).

Upon effector recognition, many tested sensor CNLs and TNLs oligomerize and undergo radical conformational changes. For example, the Arabidopsis CNL AtZAR1 and wheat CNL Sr35 form pentameric resistosomes and functions as Ca^{2+} channel to directly induce cell death and defense responses (11-15). In contrast, activated sensor TNLs form tetrameric resistosomes that are holoenzymes cleaving NAD^+ to produce small signaling molecules (16-22). These small molecules bind to the heterodimers of the Enhanced Disease Susceptibility 1 (EDS1) with either Senescence-Associated Gene101 (SAG101), or Phytoalexin Deficient4 (PAD4) and induce their association with NRG1 and ADR1, respectively (19, 20). In Arabidopsis, AtEDS1 and AtSAG101 form a stable heterodimer and cooperate with the AtNRG1s to mainly control cell death, while AtEDS1 and AtPAD4 physically associate and function with the AtADR1s to mainly mediate bacterial growth restriction, resistance and transcriptional reprogramming (6, 7, 19, 20, 23, 24), though there are some overlapping functions (8). The auto-active AtNRG1 mutant and AtADR1 were demonstrated to oligomerize and function as Ca^{2+} channel to induce cell death independent of the lipase-like proteins (3). It is currently unknown whether TNL activation is sufficient to trigger RNL oligomerization and whether EDS1/SAG101 and EDS1/PAD4 are present in NRG1 and ADR1 resistosomes, respectively.

Sensor NLRs are localized in their resting states to various places in the cell, likely in order to engage with the relevant appropriately localized effectors. Consistent with their proposed Ca^{2+} channel activities,

some activated CNLs and RNLs exhibit PM localization (3, 12-15, 25, 26). The Arabidopsis CNL RPM1 associates with the PM and remains at the PM after its activation by PM targeted effectors that modify RIN4 (25, 27). The Arabidopsis CNL RPS5 also localizes to the PM via N-terminal acylation signal and functions at the PM (26). By contrast, AtZAR1 distributes mainly in the cytoplasm in the resting state (13). Upon activation, AtZAR1 moves to, oligomerizes at and presumably protrudes through the PM to form an active Ca^{2+} channel (11, 12, 28). Plant helper NLRs including ADR1s, NRG1s and NRCs contain no predicted acylation signal but still localize at the PM before activation (3, 29, 30). AtNRG1.1 localizes to the PM, partially to ER membranes and in the cytosol when transiently over-expressed in *Nb* (3, 31). Arabidopsis ADR1s mainly localizes at the PM in a phospholipid dependent manner, since depletion of phosphatidylinositol-4-phosphate (PI4P) from the PM by overexpression of the yeast phospholipid-phosphatase Sac1p led to a mis-localization of ADR1 and loss of cell death activities (29). During activation by *Phytophthora infestans* infection, NbNRC4 accumulates at the extrahaustorial membrane (EHM) (30). When activation by sensor NLRs, NbNRC4 forms puncta mainly at the EHM and, to a lesser extent, at the PM; a constitutively autoactive NbNRC4 mutant mainly exhibits PM-associated punctate distribution, similar to autoactivated AtNRG1.1 (3, 30). Given that AtNRG1.1 CC^R cell death activity is also affected when co-expressed with the yeast phospholipid-phosphatase Sac1p (29) and that NbNRCs do also not possess any N-terminal acylation site or predicted transmembrane anchor, it is very likely that NRG1s and NRCs also associate with PM in a phospholipid dependent manner. However, how exactly the three subtypes of helper NLRs interact with phospholipids is unknown.

Here we show that the three classes of helper NLRs directly interact with phospholipids via conserved positively charged residues in the second and fourth helices of their CC^R or CC domain to anchor at the PM in both resting and active states, despite undergoing conformational changes accompanying activation. Consistent with the previously reported activation mimic AtNRG1.1 D485V (hereafter, AtNRG1.1 DV) (3, 31), effector activation of an upstream TNL induces AtNRG1.1 oligomerization and puncta formation at the PM. Interestingly, a cytoplasmic AtEDS1/AtSAG101 fraction is important for the AtNRG1.1 cell death function, but this heterodimer is absent from the oligomerized AtNRG1.1 resistosome. These results suggest that the AtEDS1/AtSAG101/AtNRG1.1 heterotrimer induced by TNL activation represents an intermediate state before dissociation of AtEDS1/AtSAG101 and subsequent oligomerization of AtNRG1.1.

Results

Positively charged residues in α4 of the 4HB contribute to NRG1 and NRC phospholipid binding and PM localization before and after activation.

We previously demonstrated that the AtADR1 CC^R domain binds to phospholipids *in vitro* (29), but it remained unknown which residues in AtADR1 CC^R were responsible for that interaction. Assuming that the ADR1 and NRG1 CC^R domains and potentially the NRC CC could use the same mechanism for phospholipid binding and PM association, we performed sequence alignment with ADR1s, NRG1s and NRCs from Arabidopsis and *Nb* to identify potential conserved, positively charged residues that might bind negatively charged phospholipids. We found an absolutely conserved lysine residue corresponding to K100 in AtNRG1.1 (Figure S1A). This lysine residue is highly conserved in ADR1s, NRG1s and NRCs across different plant species (Figure 1A). We did not observe conservation of this amino acid in AtRPS5 which features an N-terminal acylation signal for PM localization, in AtRPM1 which relies largely on association with RIN4 for PM association or in AtZAR1 which mainly localizes in the cytoplasm when overexpressed in *Nb* (Figure S1A and S1B). This observation further suggests a specific and potentially functional role for the AtNRG1.1 K100 equivalent in PM-localization of helper NLRs. Lipid-strip binding assays showed that purified AtNRG1.1 CC^R (aa 1-124) protein specifically binds to phospholipids including PI4P, while K100E completely abolished phospholipid binding (Figure 1B). K100E was still active in triggering cell death in *Nb*, though this phenotype was weaker than the control, AtNRG1.1 DV (Figure 1C). Considering that positively charged residues adjacent to K100 may also contribute to phospholipid binding and function, we mutated positively charged residues close to K100 in the α4 helix (Figure S1C). A quadruple mutant K100E/R103E/K106E/K110E (hereafter, g4m) and a penta mutant R99E/K100E/R103E/K106E/K110E (hereafter, g5m) completely suppressed the cell death activity of AtNRG1.1 DV (Figure 1C). The four single mutants including R99E, R103E, K106E and K110E showed obviously or slightly reduced binding towards phospholipids *in vitro* (Figure 1B). Both g4m and g5m strongly affected PM locations of both AtNRG1.1 WT and DV as demonstrated in Laser Confocal Microscopy (hereafter, confocal) assays, while K100E had a slight effect (Figure 1D and 1E). K100E DV and g4m DV maintained the ability to form puncta at the PM, as observed for AtNRG1.1 DV, but g5m

DV did not (Figure 1E). Blue-Native PAGE assays showed that K100E and g4m properly oligomerized in the context of AtNRG1.1 DV, while g5m oligomerization was hindered (Figure 1F, also showing equal mutant accumulation on SDS-PAGE immunoblot), consistent with the presence or absence of PM puncta in confocal assays.

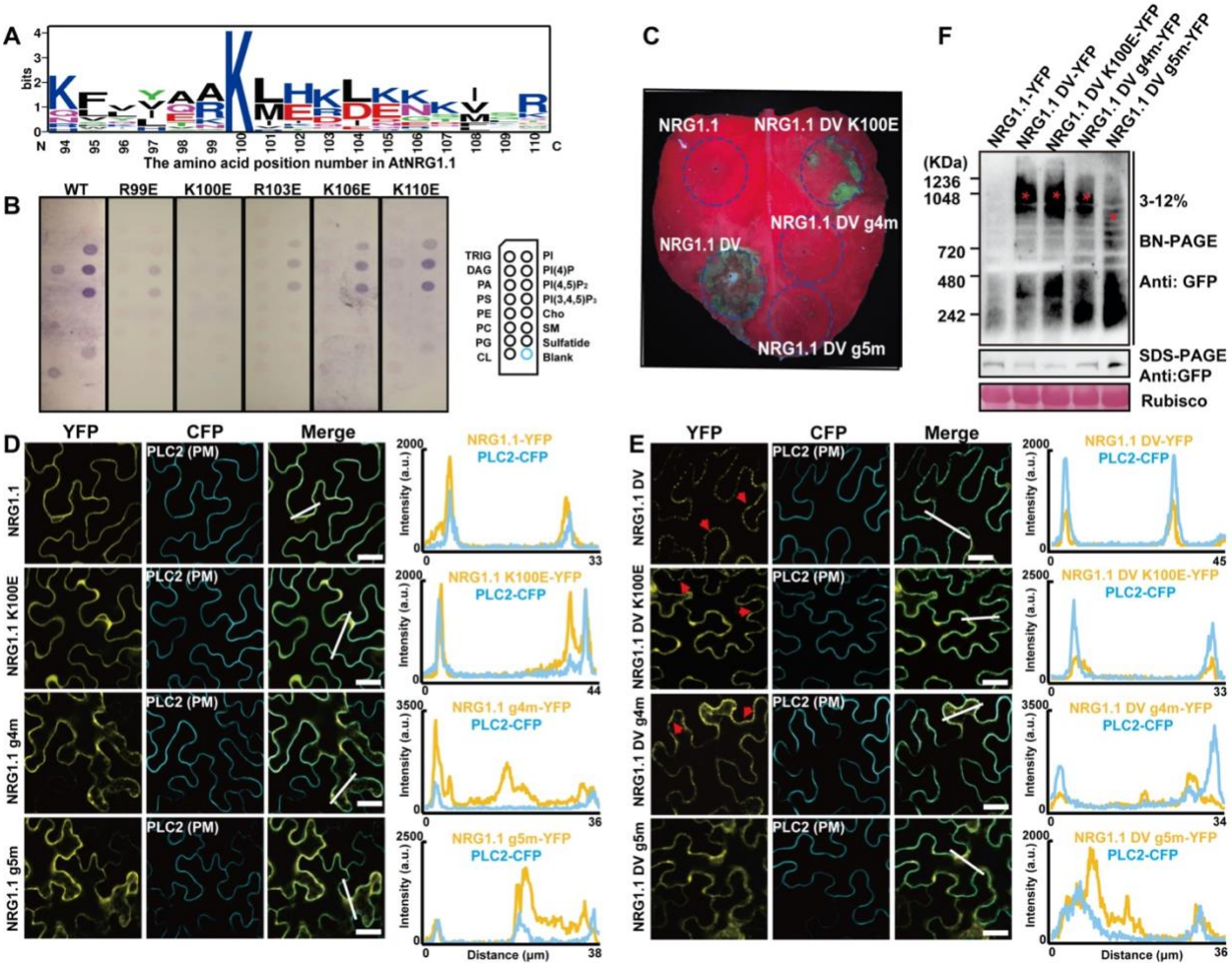

Figure 1 Positively charged residues in the α4 helix of the AtNRG1.1 4HB contribute to phospholipid binding, PM association and function. **(A)** Sequence logos showing the conservation of AtNRG1.1 K100 in three helper NLR families from different plant species. The alignment was performed with ClustalX and sequence logos were generated using WEBLOGO. **(B)** Lipid strip binding assay using purified proteins of AtNRG1.1 CC^R 1-124 and indicated mutants. See *Methods* for lipid definitions. **(C)** Cell death phenotypes of AtNRG1.1 DV and mutants with altered PM localization in *Nb* at 32h post infiltration. Confocal microscopy analyses of the mutations of the positively charged residues affecting PM localization of AtNRG1.1 **(D)** and the activation mimic allele AtNRG1.1 DV **(E)**, respectively. Confocal images are single plane secant views. Merge means merged image between YFP and CFP images. The

red head arrows indicated puncta. Fluorescence intensities were measured along the white line depicted in the merge images. Bars, 25 µm. **(E)** BN-PAGE analyses on the oligomerization of the AtNRG1.1 DV mutants with altered PM localization.

The corresponding lysine residue is not conserved generally across CNLs, but is conserved in helper NRCs including the NRC negative regulator NbNRCX (Figure S1A) (32). The conserved lysine residue in the α4 helix of the Arabidopsis RNLs corresponds to K84 in NbNRC4. K84E/K87E/K89E/K91E/R94E (hereafter, c5m) suppressed the cell death activity of NbNRC4 D478V (hereafter, NbNRC4 DV) (Figure 2A and 2B). Moreover, c5m also attenuated the PM localization of both NbNRC4 WT and NbNRC4 DV (Figure 2C and 2D), though the fluorescence signal of NbNRC4 DV was weak because of cell death starting from 24h post infiltration. NbNRCX exhibited strong PM localization, while K84E/K89E/K92E/K93E (hereafter, x4m) exhibited reduced PM localization (Figure 2E). Hence, the positively charged residues in α4 helix of the 4HB contribute to NRG1 and NRC phospholipid binding and PM localization before and after activation, suggesting a conserved mechanism.

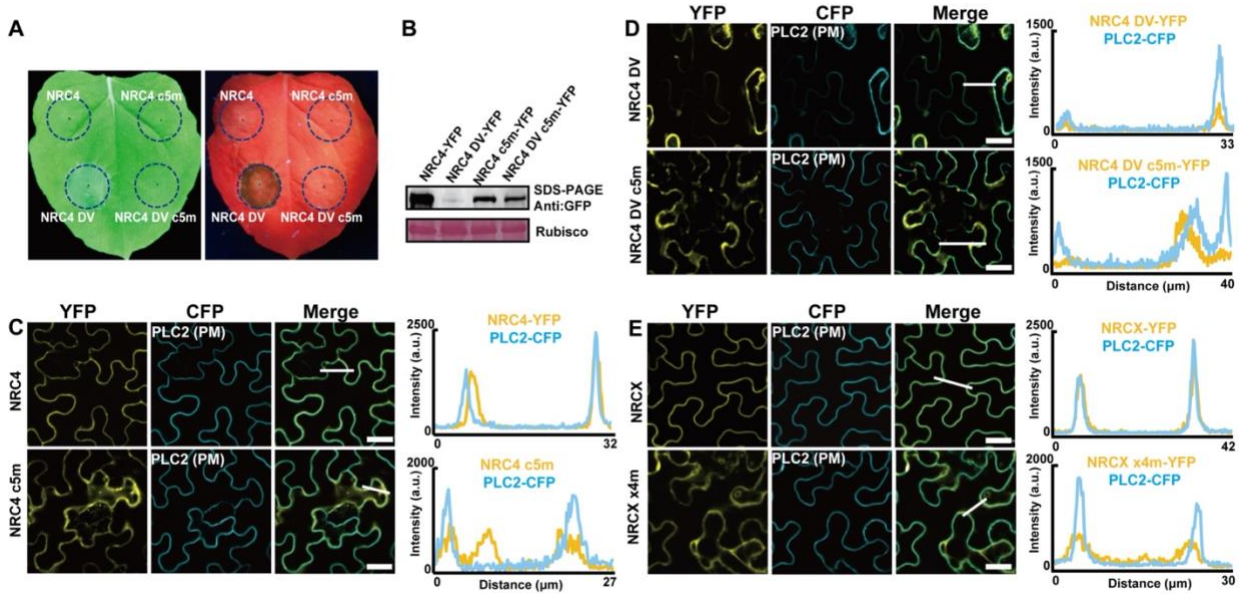

Figure 2 Mutations of the positively charged residues in the α4 helix of the 4HB affect NbNRC PM localization and function. **(A)** Cell death phenotypes of an NbNRC4 DV activation mimic and mutants with altered PM localization in *Nb* 32h post infiltration. Confocal microscopy analyses of the mutations of the positively charged residues affecting PM localizations of NbNRC4 **(B)**, NbNRC4 DV **(C)**, and NbNRCX **(D)**, respectively. The indicated proteins fused with a C-terminal YFP were transiently co-

expressed with the PM marker PLC2 fused to CFP in *Nb* leaves and confocal images were taken at 32-36h post infiltration. Images are single plane secant views. Merge means merged images between YFP and CFP images. Fluorescence intensities were measured along the white line depicted in the merge images. Bar, 25 µm.

Positively charged residues in the α2 and α4 helices of 4HB collectively affect ADR1 PM localization before and after activation

Mutations in the α4 helix of the 4HB abolished the cell death function of AtNRG1.1 DV and NbNRC4 DV, but only partially affected PM localization, indicating that additional residues may also contribute to phospholipid binding. To further investigate if additional residues indeed contribute to phospholipid binding, we chose to focus on AtADR1-L1 because of its distinct PM localization compared to AtNRG1.1 and NbNRC4 (29). The conserved lysine residue in the α4 helix corresponds to K99 in AtADR1-L1. The quadruple mutant R98, K99, K102, K105 (hereafter, r4m) in α4 strongly attenuated AtADR1-L1 D489V (hereafter, AtADR1-L1 DV) cell death activity (Figure 3A, with protein accumulation controls in S2A) and affected the PM localization of both AtADR1-L1 WT and AtADR1-L1 DV (Figure 3B and 3C). Further search for conserved positively charged residues in the 4HB of RNLs identified a highly conserved K or R residue corresponding to K30 in AtADR1-L1 and K35 in AtNRG1.1 (Figure S1A and 3D), and the corresponding positions in NRCs are also largely conserved (Figure S1A). A triple mutant of K30 and adjacent positively charged residues, R28E/K30E/K34E (hereafter, r3m), suppressed the cell death phenotype of AtADR1-L1 DV (Figure 3A), suggesting a critical role of the positively charged residues in the α2 helix. Confocal assays further demonstrated that r3m affected the PM localization of both AtADR1-L1 WT and DV, while the combination of r3m and r4m dramatically reduced the PM localization of both AtADR1-L1 WT and DV to be largely cytoplasmic (Figure 3B and 3C). Based on an AlphaFold structure model of AtADR1-L1 CC^R in the resting state, the two clusters of positively charged residues involved in r3m and r4m are spatially close to each other (Figure S2B). Hence, the α2 and α4 helices collectively contribute to phospholipid binding and PM localization of ADR1 before and after activation.

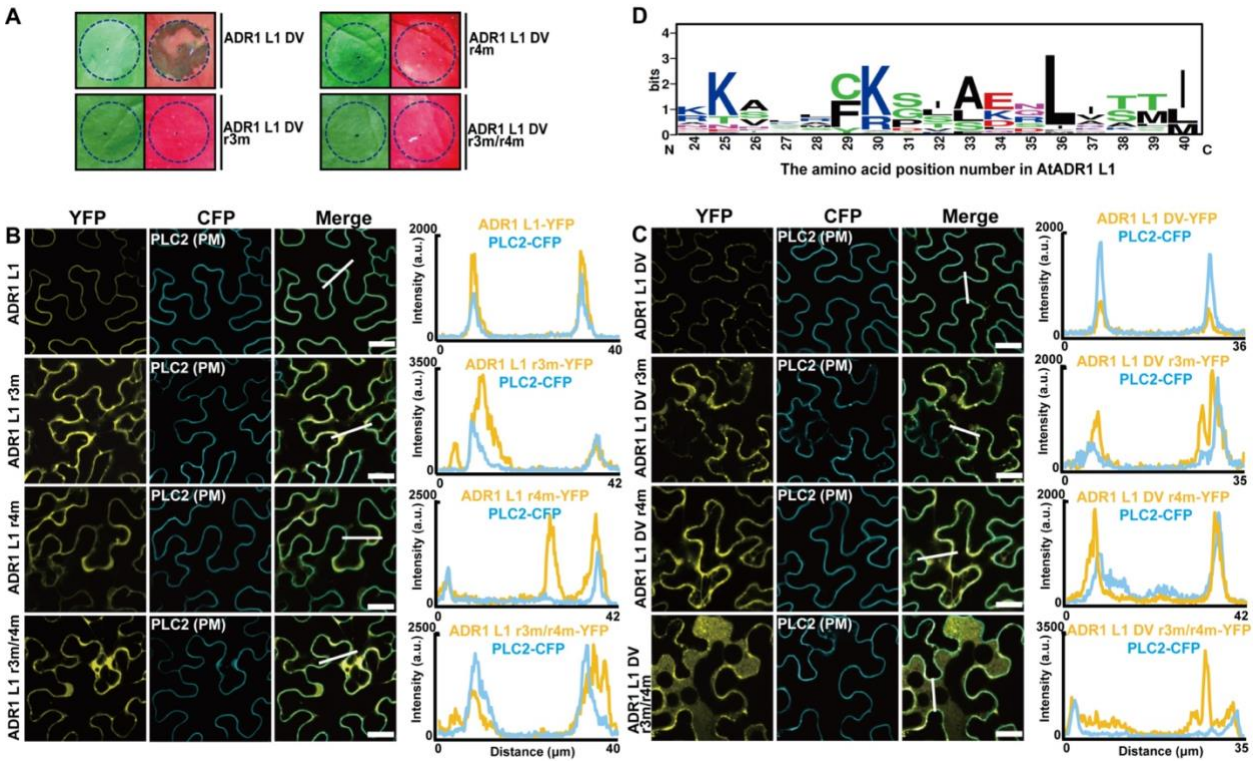

Figure 3 Positively charged residues in the α2 an α4 helices of the 4HB collectively contribute to AtADR1_L1 PM localization and function. **(A)** Cell death phenotypes of AtADR1_L1 DV and mutants with altered PM localization in *Nb* 32h post infiltration. Confocal microscopy analyses of the mutations of the positively charged residues affecting PM localizations of AtADR1_L1 **(B)** and AtADR1_L1 DV **(C)**, respectively. Confocal images are single plane secant views. Merge means merged image between YFP and CFP images. The red head arrows indicated puncta. Fluorescence intensities were measured along the white line depicted in the merge images. Bars, 25 µm. **(D)** Sequence logos showing the conservation of AtADR1_L1 K30 in RNLs from different plant species. The alignment was performed with ClustalX and sequence logos were generated using WEBLOGO.

Our data indicate that these helper NLRs are localized to the PM in the resting state via the positively charged residues in the α2 and α4 helices of the 4HB that interact with phospholipids. According to the AtZAR1 activation model, the α1 helix flips out of the 4HB and inserts into the PM upon activation (13) (Figure S2C). The conserved positively charged residue in the α2 helix corresponding to K30 in AtADR1-L1 is located at the very beginning α2 (Figure S2B) and could still associate with the PM following an AtZAR1-like activation model (Figure S2C). Also, the α4 helix becomes disordered upon oligomerization

but maintains contact with the PM (13) (Figure S2C). These conformational changes are likely to allow positively charged amino acids in the α2 and α4 helices to maintain association with the PM post activation. Hence, helper NLRs rely on the conserved positively charged residues in both the α2 and α4 helices of the 4HB for phospholipid binding and PM localization before and after activation, despite the conformational changes generated by activation.

Effector activation of a TNL induces AtNRG1.1 resistosome formation at the PM

Our previous study on auto active AtNRG1.1 DV used different loss-of-function mutations, including L134E that abolished oligomerization, ΔN16 (deletion of residues 2-16) that enhanced oligomerization and D3N/E14Q that specifically blocked Ca^{2+} channel activity (3). It remained unknown whether AtNRG1.1 indeed oligomerizes at the PM following activation by an effector and its corresponding TNL. We transiently expressed AtEDS1/AtSAG101/AtNRG1.1 in *Nb epss* (*eds1a, pad4, sag101a, sag101b*) leaves (6) together with the effector XopQ to reconstitute the TNL Roq1 cell death phenotype (33). AtNRG1.1 WT, but not L134E, ΔN16, D3N/E14Q or g4m, caused cell death (Figure 4A). We employed Blue-Native PAGE to investigate AtNRG1.1 oligomerization status following effector activation. AtNRG1.1 WT, ΔN16, D3N/E14Q and g4m oligomerized following Roq1 activation by XopQ, with ΔN16 exhibiting much stronger oligomerization signal than the others; L134E failed to oligomerize (Figure 4B). Hence, g4m specifically affects PM localization of AtNRG1.1, but not oligomerization (Figure 1D, 1E and 1F). These cell death phenotypes and oligomerization states are consistent with observations using the activation mimic allele AtNRG1.1 DV (Figure 1C, 1F, and 4B) (3). In confocal assays, AtNRG1.1 WT, D3N/E14Q and g4m, which all maintained the ability to oligomerize, also exhibited puncta close to or on the PM, and ΔN16 displayed enhanced puncta; the loss-of-oligomerization mutant L134E exhibited no obvious puncta formation compared to AtNRG1.1 WT (Figure 4C-4G). These data demonstrate that effector activation of a TNL induces AtNRG1.1 resistosome formation at the PM and that AtNRG1.1 DV faithfully mimics the functionality of effector activated AtNRG1.1.

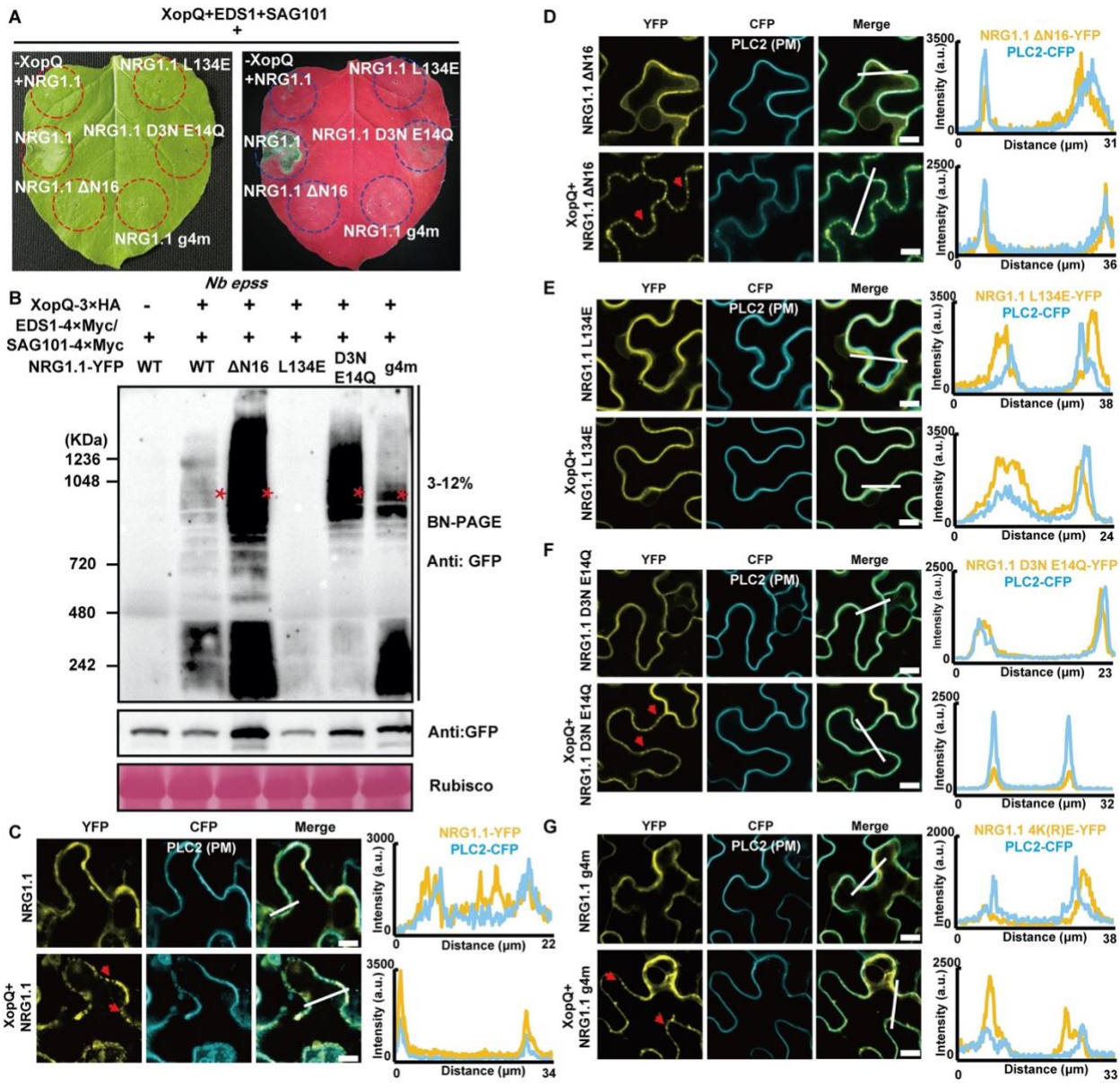

Fig. 4 Effector induces AtNRG1.1 oligomerization and enhanced puncta formation at the PM. **(A)** XopQ-triggered cell death phenotypes in *Nb epss* when co-expressed with AtEDS1, AtSAG101 and AtNRG1.1 mutants 48h post infiltration. **(B)** BN-PAGE showing the oligomerization status of AtNRG1.1 mutants in (A). Red asterisks indicate oligomerized AtNRG1.1. Confocal microscopy assays showing PM localization and puncta of AtNRG1.1 **(C)**, derivative alleles ΔN16 **(D)**, L134E **(E)**, D3N/E14Q **(F)** and g4m **(G)** before and post-activation via XopQ expression when co-expressed with AtEDS1 and AtSAG101. Images are single plane secant views. Merge means merged images between YFP and CFP images. Fluorescence intensities were measured along the white line depicted in the merge images. Bar, 10 μm.

The cytoplasmic pools of AtEDS1 and AtSAG101 mediate cell death but are not present in the oligomerized AtNRG1.1 resistosome

AtEDS1 and AtSAG101 are localized to the nucleus and the cytoplasm (34, 35). We investigated whether enforced nuclear and cytoplasmic distribution of AtEDS1 and AtSAG101 could affect the cell death phenotype using co-expression complementation assays in *Nb epss* plants. Expression of AtEDS1 and AtSAG101 with a nuclear export signal (NES) supported XopQ-TNL Roq1 dependent cell death comparable to wild type AtEDS1 and AtSAG101. By contrast, AtEDS1 and AtSAG101 with a nuclear localization signal (NLS) did not support cell death in this assay (Figure 5A and S3). These data suggest that the cytoplasmic pools of AtEDS1 and AtSAG101 activate AtNRG1.1 and are the major determinants of XopQ-activated cell death responses. Given that TIR-dependent signals induce the formation of AtEDS1/AtSAG101/AtNRG1 heterotrimers (20), we performed BN-PAGE to further investigate if AtEDS1 and AtSAG101 are subsequently retained in the oligomerized AtNRG1.1 resistosome. AtNRG1.1 ΔN16 oligomerized in a XopQ-dependent manner following activation of the Roq1 TNL when co-expressed with AtEDS1 and AtSAG101, while AtNRG1.1 ΔN16/L134E was not responsive to XopQ (Figure 5B and S5). However, in samples expressing AtNRG1.1 ΔN16, with or without XopQ, or AtNRG1.1 ΔN16/L134E plus XopQ, we did not detect oligomerization of AtEDS1 (Figure 5B, StrepII immunoblot) or AtSAG101 (Figure 5B, FLAG immunoblot) at the high molecular weight regions corresponding to AtNRG1.1 oligomers. We ruled out the tag effect for the negative results by detecting oligomerization of AtRNG1.1 ΔN16 with the same epitope tag as either AtEDS1 or AtSAG101 in a single gel at three different time points 26h, 32h, and 42h post infiltration (Figure 5B and S5). These data indicate that AtEDS1 and AtSAG101 are not present in the oligomerized AtNRG1.1 resistosome. Our results also suggest that additional signals may be required to trigger the dissociation of AtEDS1/AtSAG101 and subsequent oligomerization of AtNRG1.1 after TIR-induced AtEDS1/AtSAG101/AtNRG1.1 heterotrimer formation (Figure 5C).

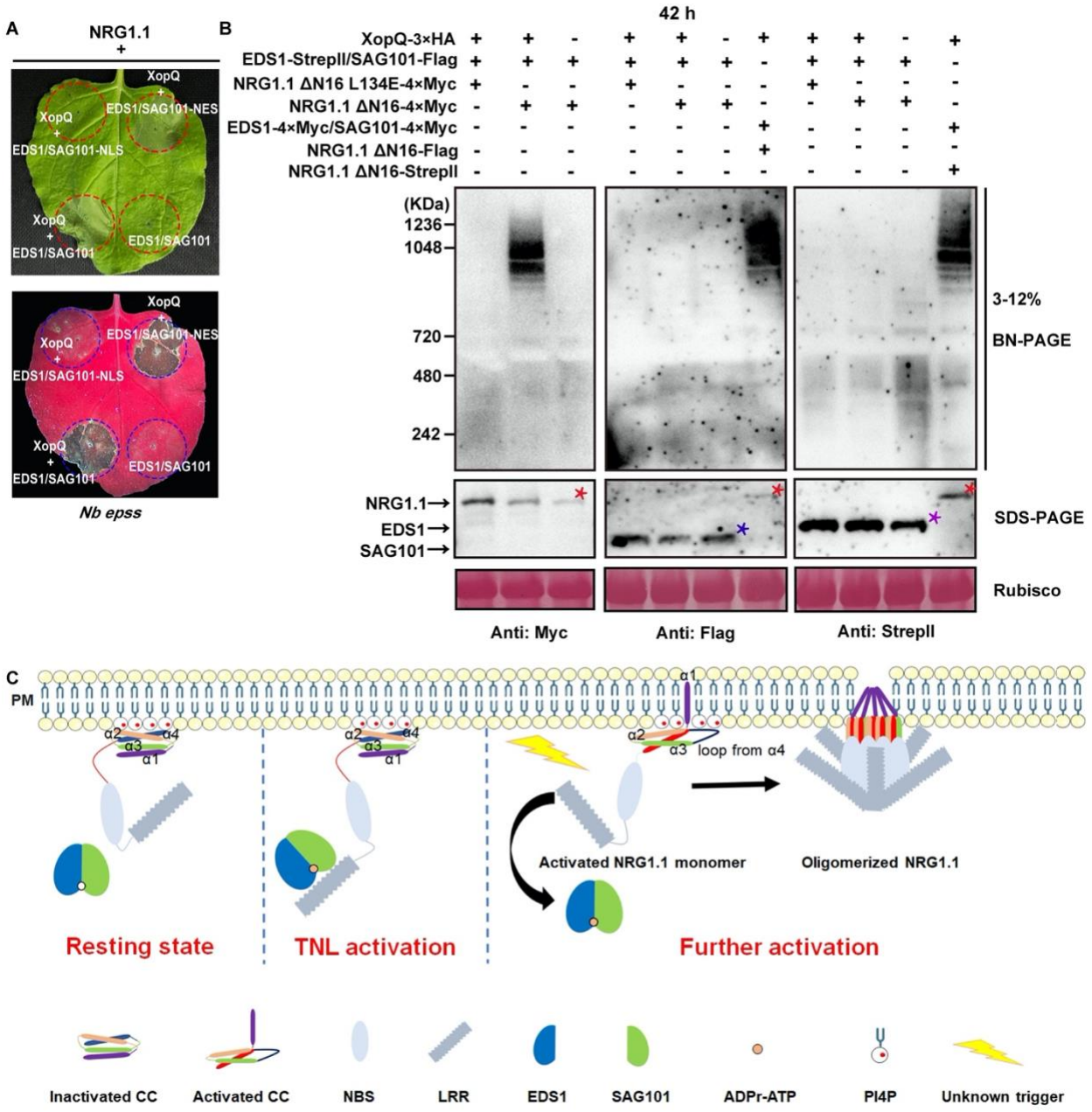

Fig. 5 AtEDS1 and AtSAG101 are not present in the oligomerized AtNRG1.1 resistosome. **(A)** The cytoplasmic pool of EDS1/SAG101 activates NRG1.1 to induce cell death. EDS1/SAG101-NLS, EDS1/SAG101-NES, or EDS1/SAG101 with a C-terminal YFP-HA tag were transiently co-expressed with NRG1.1-4×Myc and XopQ-4×Myc in *Nb epss*. Cell death phenotypes were photographed 42h post infiltration. **(B)** EDS1/SAG101 do not co-migrate with NRG1.1 upon XopQ activation in BN-PAGE assays. *Agrobacteria* mixes carrying the indicated expression constructs were co-infiltrated into *Nb epss*. Total protein extracts were resolved by BN-PAGE and SDS-PAGE 42h post infiltration. Target bands

were immunoblotted with appropriate antibodies. Red asterisk indicates the protein band of NRG1.1. Purple and blue asterisks indicate EDS1 and SAG101 bands, respectively. **(C)** An updated model on PM association and effector-induced oligomerization of NRG1.

Discussion

PM localization was required for Ca^{2+} channel formation or immune function of RNLs and many CNLs (3, 12, 14, 15, 25, 26, 29, 30). Helper NLRs, including NRG1s and ADR1s, exhibited significant PM location before activation (or the extra-haustorial membrane in the case of NbNRC4) and are further enriched and concentrated at the PM after activation (3, 29-31). Mechanisms driving helper NLR PM localization remained largely unclear.

In plants, PI4P is the main driver of PM electrostatics (36, 37). Phosphatidic acid (PA) and phosphatidylserine and PI(4,5)P_2 also contribute to PM (inner leaflet) surface charges, but to a lesser extent. We generated mutations in the conserved positively charged residues in the α2 and α4 helices of helper NLR 4HBs. These mutations attenuated phospholipid binding *in vitro* and PM association *in vivo*; they also abolished cell death function. Another 4HB-containing membrane pore forming protein, the animal mixed lineage kinase domain-like (MLKL), specifically interacts with phospholipids for PM localization and function (38). A recent study showed that *Mycobacterium tuberculosis* inhibits pyroptosis by secreting a phospholipid phosphatase that localizes at the host PM to dephosphorylate PI4P and PI(4,5)P_2 and suppresses the PM association and pore function of activated Gasdermin D (39). Hence phospholipid-binding mediated PM association is a conserved mechanism for membrane pore forming proteins. It remains to be investigated whether plant pathogens employ similar phospholipid phosphatases to perturb the PM localization and thus the function of helper NLRs.

We provide mechanistic insights into the dynamics of PM association during plant helper NLR activation. In the absence of pathogen infection, interactions of the α2 and α4 helices of the N-terminal 4HB anchor a significant fraction of plant helper NLRs at the PM. Upon activation by senor NLRs, helper NLRs undergo dramatical conformational changes and further concentration at the PM; they still rely on the α2 and α4 helices to associate with the PM for function (Figure 5C).

The RNL helper ADR1s and NRG1s contain an RPW8-like CC^R domain at their N-termini. In addition to the 4HB, the CC^R domain has an extra N-terminal region that was previously predicted to be responsible for CC^R membrane targeting (40). Deletion of the extra N-terminal region did not affect PM localization of the activation mimic allele AtNRG1.1 DV (3) or effector-activated AtNRG1.1 (Figure 4D). Mutation of the positively charged residues in the α4 helix affected PM localization of AtNRG1.1 WT and the DV allele (Figure 1D and 1E). Despite the absolute conservation of AtNRG1.1 K100 in the CC^R domain of ADR1s and NRG1s, it is not conserved in RPW8 (Figure S1A), indicating a different PM association mechanism for RPW8.

AtNRG1.1 K100 is highly conserved in RNL and NRC helpers, but is less well conserved in sensor CNLs (Figure S1A). In contrast to RNL helpers, the well-studied sensor CNL AtZAR1 that also functions as a PM-localized Ca^{2+} channel post activation, localizes mainly in the cytoplasm before activation (Figure S1B) (12, 13). In contrast, the sensor CNL AtRPM1 interacts with the PM-localized guardee RIN4, localizes to and signals from the PM (25, 41, 42); the senor CNL AtRPS5 localizes to the PM via N-terminal acylation signal and functions at the PM (26). Thus, sensor NLRs express variable resting state subcellular distributions, likely reflecting the subcellular localization of the pathogen effectors they detect. Hence, helper NLR use a specific mechanism for enrichment at the PM before activation, which may be critical for rapid calcium signal activation upon activation of ETI. It remains to be determined whether other CNLs also use similar phospholipid binding mechanisms to determine or enhance PM localization.

PTI and ETI function cooperatively and potentiate each other (43, 44), but the mechanisms that interconnect PTI and ETI remain unclear. The EDS1/PAD4/ADR1 module associates with some PM located PRRs and is required for PTI (45-47). NbNRC3 mediates the hypersensitive cell death caused by the cell-surface receptor Cf-4 recognizing the apoplastic fungal effector Avr4 (48). An enriched or constitutive PM-bound pool of helper NLRs are potentially important for their efficient activation by PTI signals and the cooperative function between PTI and ETI. We also demonstrated that NbNRCX, a negative regulator of NbNRC2 and NbNRC3 (32), also uses the conserved positively charged residues in the α4 helix of 4HB for PM association (Figure 2D). We propose that the PM location of NbNRCX is

important for its negative regulation of activated NbNRC2 and NbNRC3 at the PM, perhaps via the formation of mixed and thus 'poisoned' oligomers.

Effector activation of sensor CNL triggers helper NRC oligomerization, and sensor CNLs are not present in the NRC oligomer complex (49, 50). We present data that ETI activated via the effector XopQ and the TNL Roq1 induces the RNL AtNRG1.1 oligomerization and puncta formation at the PM (Figure 4). A recent study showed that oligomerization of AtNRG1.2 requires not only effector-mediated activation of a TNL but also activation of PTI (51). Our data show that the cytoplasmic pool of AtEDS1/AtSAG101 mediates the cell death response, but are not present in the oligomerized AtNRG1.1 resistosome (Figure 5A and 5B). These data suggest that additional unknown triggers are required to induce AtEDS1/AtSAG101 dissociation from the AtNRG1.1/AtEDS1/AtSAG101 heterotrimer and subsequent AtNRG1.1 oligomerization or that the conformational changes resulting from oligomerization abrogate the interface for AtEDS1/AtSAG101 association (Figure 5C). The putative role of PTI in facilitating oligomeric NRG1 resistosome formation at the PM requires future investigation.

Materials and methods

Plant growth conditions

Nb WT and *Nb epss* plants were grown in a growth chamber at 25°C under a 16 h/8 h light/dark cycle with relative humidity at 55±10%.

Vector construction

The coding sequences (CDS) of *AtNRG1.1* (At5g66900), *AtEDS1* (At3g48090), *AtSAG101* (At5g14930), *AtADR1-L1* (At4g33300) and *PLC2* (At3g08510) were amplified using specific primers from the Arabidopsis ecotype Col-0, and the CDS of *NbNRC4* (NbS00016103g0004, 2,464 bp) and *NbNRCX* (NbS00030243g0001, 2,619 bp) were amplified by PCR from *Nb*. The resulting PCR fragments were cloned into a modified pUC19 vector with the gateway compatible recombination sites (attL1/attL2). The StrepII tag sequence was fused to the 3' cDNA of *AtEDS1* to obtain an *AtEDS1-StrepII* entry clone. *AtNRG1.1 ⊿16* was PCR-amplified using the CDS of *AtNRG1.1* as a template and then cloned into the entry vector pUC19. Other *AtNRG1.1* variants were generated using Fast Mutagenesis System protocol (Transgene). *XopQ* with *attL1/attL2* sequences was synthesized into a pUC18 plasmid (Genescript). *XopQ* was introduced to expression vectors pGWB614 and pGWB617 to obtain *35S:: XopQ-3×HA* and *35S:: XopQ-4×Myc* constructs, respectively. *AtEDS1* and *AtEDS1-StrepII* were recombined into pGWB617 (35S promoter, C-terminal 3×Myc) and pGWB2 (35S promoter, no tag), respectively. *AtSAG101* was introduced to pGWB11 (35S promoter, C-terminal Flag) and pGWB617. *AtNRG1.1* and the mutants were introduced into pGWB641 (35S promoter, C-terminal EYFP), pGWB617, the modified vectors pEarleyGate-Flag (35S promoter, C-terminal Flag) and pEarleyGate-StrepII (35S promoter, C-terminal StrepII) to express fusion proteins with desired tags. All target sequences were introduced into expression vectors using LR reactions (Life Technologies). *35S::AtEDS1-YFP-HA-NLS* (or *NES*) and *35S::AtSAG101-YFP-HA-NLS* (or *NES*) expression constructs were obtained using LR to recombine pUC19-*AtEDS1*, pUC19-*AtSAG101* with modified vectors pEarleyGate 101-NLS and pEarleyGate 101-NES (52). *NbNRC4* and *NbNRCX*, and their mutants were introduced into the 35S-omega-driven destination vector pEarlyGate with a C-terminal YFP-HA. The obtained expression constructs were transformed into *Agrobacterium tumefaciens* GV3101 via electroporation for transient expression in *Nb*.

Transient expression in *Nb*

Agrobacteria (GV3101) carrying the constructs were grown overnight in LB with suitable antibiotics. 3 mL of *Agrobacterium* culture was centrifuged and resuspended in MES buffer (10 mM $MgCl_2$, 10 mM MES pH 5.6, 150 μM acetosyringone). *Agrobacteria* were incubated at room temperature for 1h and infiltrated into the leaves of 5-week-old *Nb or Nb epss* at specific OD_{600} values. *Agrobacteria* containing the *P19* construct was co-infiltrated at OD of 0.1. Cell death phenotypes were photographed at indicated time point.

Total protein extraction and western blot analysis

Three 8 mm leaf discs were harvested and ground to powder in liquid nitrogen. Total protein was extracted with 100 μL extraction buffer (20 mM Tris–HCl pH 8.0, 5 mM EDTA, 1% SDS, 10 mM DTT). Lysate was boiled at 95 °C with 1×protein loading buffer for 10 min. The total protein extract was cleared by centrifuge at 13,000 *g* for 10 min. Then the supernatant was separated by 10% SDS–PAGE gels and detected with corresponding antibodies. Antibodies used for immunoblotting include anti-GFP (#G1544, Sigma), anti-HA (#11867423001, Roche), anti-Myc (#M4439, Sigma), anti-Flag (#SAB4301135, Sigma), anti-StrepII (#ab76949, Abcam), and HRP-conjugated antibodies (#IMR-GtxMu-003-DHRPX, #IMR-GtxRb-003-DHRPX, #GtxRt-003-DHRPX, Jackson).

BN-PAGE

BN-PAGE was performed as previously described with slight modifications (3). 3 leaf disks (5 mm diameter) were homogenized with liquid nitrogen. 1× NativePAGE™ Sample Buffer (BN2008, Invitrogen™) with 1× protease inhibitor cocktail was added to the homogenized samples. The mixed samples were centrifuged at 20,000 *g* for 30 min at 4°C. Native PAGE™ 5% G-250 Sample Additive (BN2004, Invitrogen™) was added to the supernatant at a final concentration of 0.125%. Proteins were separated by Native PAGE™ Novex® 3–12% Bis-Tris Gels (BN1001, Invitrogen™) and transferred to PVDF membrane using an eBlot™ L1 transfer system (GenScript). The target proteins were probed with corresponding antibodies.

Confocal microscopy analyses

For *Agrobacterium*-mediated transient expression in *Nb*, OD_{600} cultures were adjusted to 0.1 of P19, 0.2 of PLC2, and 0.2 of AtNRG1.1, AtADR1-L1, NbNRC4 or NbNRCX. *Agrobacteria* mixtures were infiltrated into young leaves of 4-6 weeks old *Nb* plants. For transient expression in *Nb epss*, the OD_{600} was adjusted to 0.1 of P19, 0.1 of AtEDS1 and AtSAG101, and 0.2 of AtNRG1.1 and PLC2, and 0.001 for XopQ. Agrobacteria mixtures were infiltrated into young leaves of 4-6 weeks old *Nb epss* plants. Leaves were imaged for protein localization analyses between 36h-48h post infiltration. Confocal images were taken on a confocal laser scanning microscope LSM880 from Zeiss (Oberkochen, Germany) using the ZENblack software, via a Zeiss-C-Apochromat 20×/0.8 A20650-9901 objective or a Zeiss-W-Plan-Apochromat 421462-9900 objective. YFP was excited using a 514 nm laser and the emission spectrum was between 516-556 nm; CFP was excited with a 458 nm laser and the emission spectrum was between 463-513 nm. Focal plane images were processed with the ZEN blue software (Zeiss) for adjustment of brightness and contrast.

Sequence alignment of helper NLR homologs

AtNRG1.1 and AtNRG1.2 (At5g66910.1) were used to identify NRG1 homologs in the predicted protein databases including Solanaceae Genomics Network (SGN) and Integrated Microbial Genomes (IMG). Similarly, AtADR1 (At1g33560.1), AtADRL1-L1 and AtADRL1-L2 (At5g04720.1 were used to identify ADR1 homologs. NbNRC2 (NbS00018282g0019.1 and NbS00026706g0016.1), NbNRC3 (NbS00011087g0003.1), NbNRC4 (NbS00002971g0007.1 and NbS00016103g0004.1) and NbNRCX (NbS00030243g0001.1) were used to identify NRC-helper clade homologs in the SGN database. Top hits from BLASTP search results in different plant species were collected for further analyses. Homologs with protein sequence identity of more than 50% were aligned in their CC or CC^R domains by CLustalW. The gene ID of homologs used in the alignment were listed in Table S1.

Sequence logos visualization

Sequence logos of the identified conserved amino acid site in CC or CC^R domain of helper NLRs were generated by the online software WEBLOGO (http://weblogo.berkeley.edu/logo.cgi) (53).

Protein expression and Lipid-strip binding assays

Sequences of AtNRG1.1 CC 1-124 (WT, R99E, K100E, R103E, K106E and K110E) were subcloned into the pET24a plasmid with a N-terminal 6×His and a C-terminal StrepII tag. Proteins were expressed in *E. coli* BL21 (DE3) cells using the autoinduction method (54). Cell pellets were resuspended and lysed in buffer containing 50 mM HEPES (pH 8.0), 300 mM NaCl, 2 mM DTT and 1 mM PMSF. After sonication and centrifugation at 20,000 *g* for 60 minutes, supernatant was loaded onto a nickel HisTrap 5 mL column (GE Healthcare) pre-equilibrated with 20 mL of the wash buffer (50 mM HEPES pH 8.0, 300 mM NaCl, 30 mM imidazole) at a 3 mL/min rate. The bound proteins were eluted with elution buffer (50 mM HEPES pH 7.5, 300 mM NaCl, 500 mM imidazole), and further purified using size exclusion chromatography (Superdex 200 HiLoad 16/600 column) pre-equilibrated with the buffer containing 10 mM HEPES pH 7.5, 150 mM NaCl and 1mM DTT. The peak fractions were confirmed by SDS-PAGE and concentrated to a final concentration of 10 mg/mL for Lipid-strip binding assays.

Lipid-strip binding assays were performed according to the manufacturer's instructions (Echelon Biosciences, Salt Lake City, UT, USA). Briefly, the PIP-strip membranes were blocked overnight at 4 °C in blocking buffer containing 0.1% Tween-20 and 4% fatty acid-free bovine serum albumin in PBS buffer. Purified proteins (0.5 μg/mL, final concentration) were incubated with the PIP-strip membranes for 1 h at room temperature and then washed three times using wash buffer containing 0.1% Tween-20 in PBS buffer. Bound proteins were detected by immunodetection of StrepII. Lipids in the strip include phosphatidylinositol (4)-phosphate (PI(4)P), phosphatidylinositol (4,5)-bisphosphate (PI(4,5)P2), phosphatidylinositol (3,4,5)-trisphosphate (PI(3,4,5)P3), triglyceride (TRIG), diacylglycerol (DAG), phosphatidic acid (PA), phosphatidylserine (PS), phosphatidylethanolamine (PE), phosphatidylcholine (PC), phosphatidylglycerol (PG), cardiolipin (CL), phosphatidylinositol (PI), cholesterol (Cho), sphingomyelin (SM) and 3-sulfogalactosylceramide (Sulfatide).

Acknowledgments

We thank the confocal microscopy facility at CAS Ecology/Center for Excellence in Molecular Plant Sciences for technical supports. L.W. was supported by National Key Laboratory of Plant Molecular Genetics, Institute of Plant Physiology and Ecology/Center for Excellence in Molecular Plant Sciences and Chinese Academy of Sciences Strategic Priority Research Program (Type-B;

Project number: XDB27040214). X.L. was supported by a Postdoc Grant (Project number: 2021M693172) from National Natural Science Foundation of China. F.EK. is supported by the German Research foundation (DFG Grants CRC1101 D09 and EL 734/3-1). J.L.D. is supported by National Science Foundation (Grant IOS-1758400) and HHMI. J.L.D. is a Howard Hughes Medical Institute (HHMI) Investigator. This article is subject to HHMI's Open Access to Publications policy. HHMI lab heads have previously granted a nonexclusive CC BY 4.0 license to the public and a sublicensable license to HHMI in their research articles. Pursuant to those licenses, the author-accepted manuscript of this article can be made freely available under a CC BY4.0 license immediately upon publication.

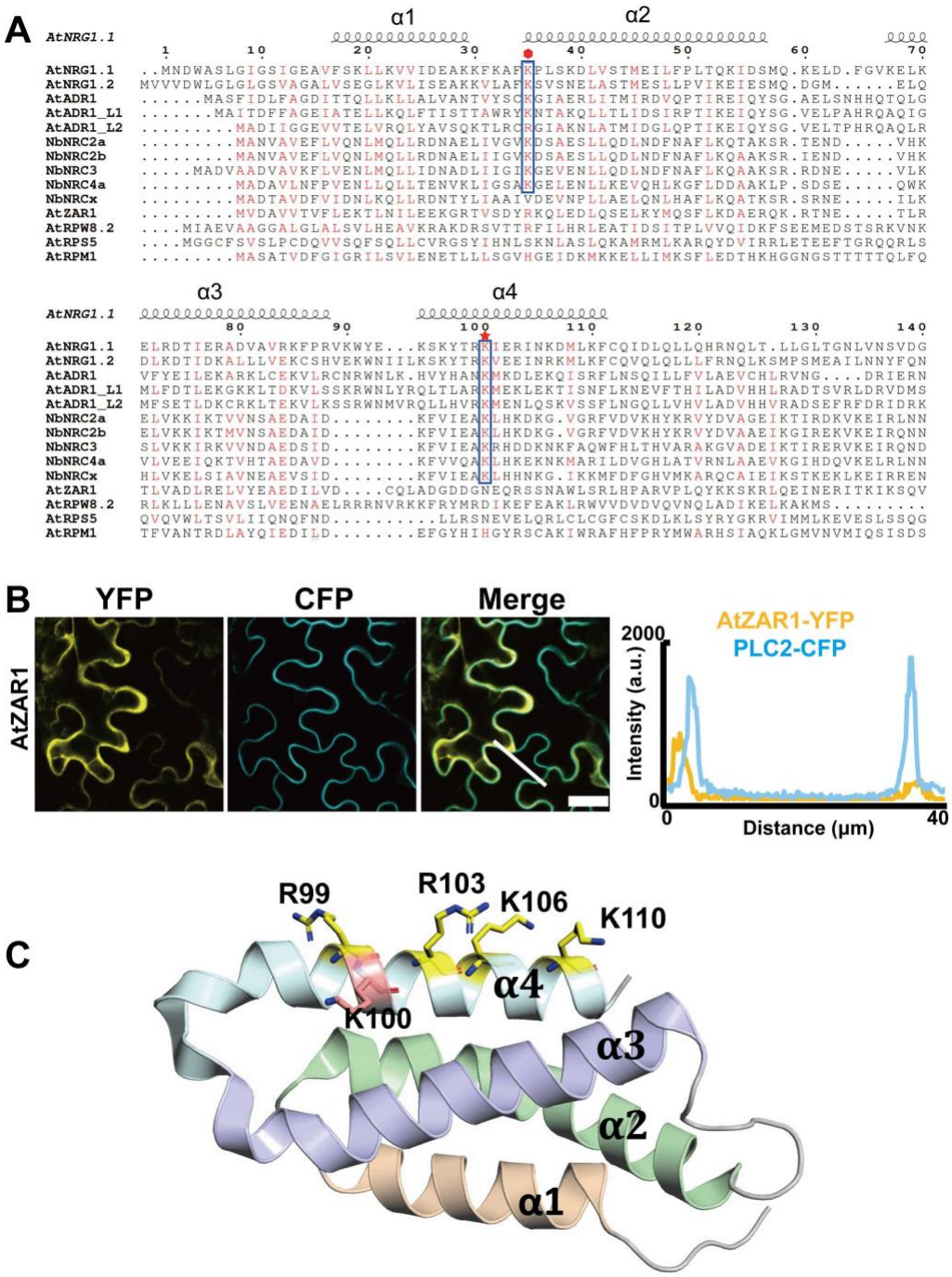

Figure S1 Identification of conserved positively charged residues in plant helper NLRs. **(A)** Sequence alignment in the CC^R and CC domains of helper NLRs and some sensor CNLs from Arabidopsis and *Nb*. The alignment was performed with ClustalX and the figure was prepared using ESPript. Red asterisk points to the position of AtNRG1.1 K100, and red hexagon points to the position of AtADR1_L1 K30. **(B)** Confocal assay showing that resting state AtZAR1 mainly

localizes in the cytosol. Fluorescence intensities were measured along the white line depicted in the merge images. Bars, 25 µm. **(C)** Cartoon presentation of AtNRG1.1 CC^R structure (PDB:7L7W) with R99 K110, R103, K106 and K110 shown as sticks.

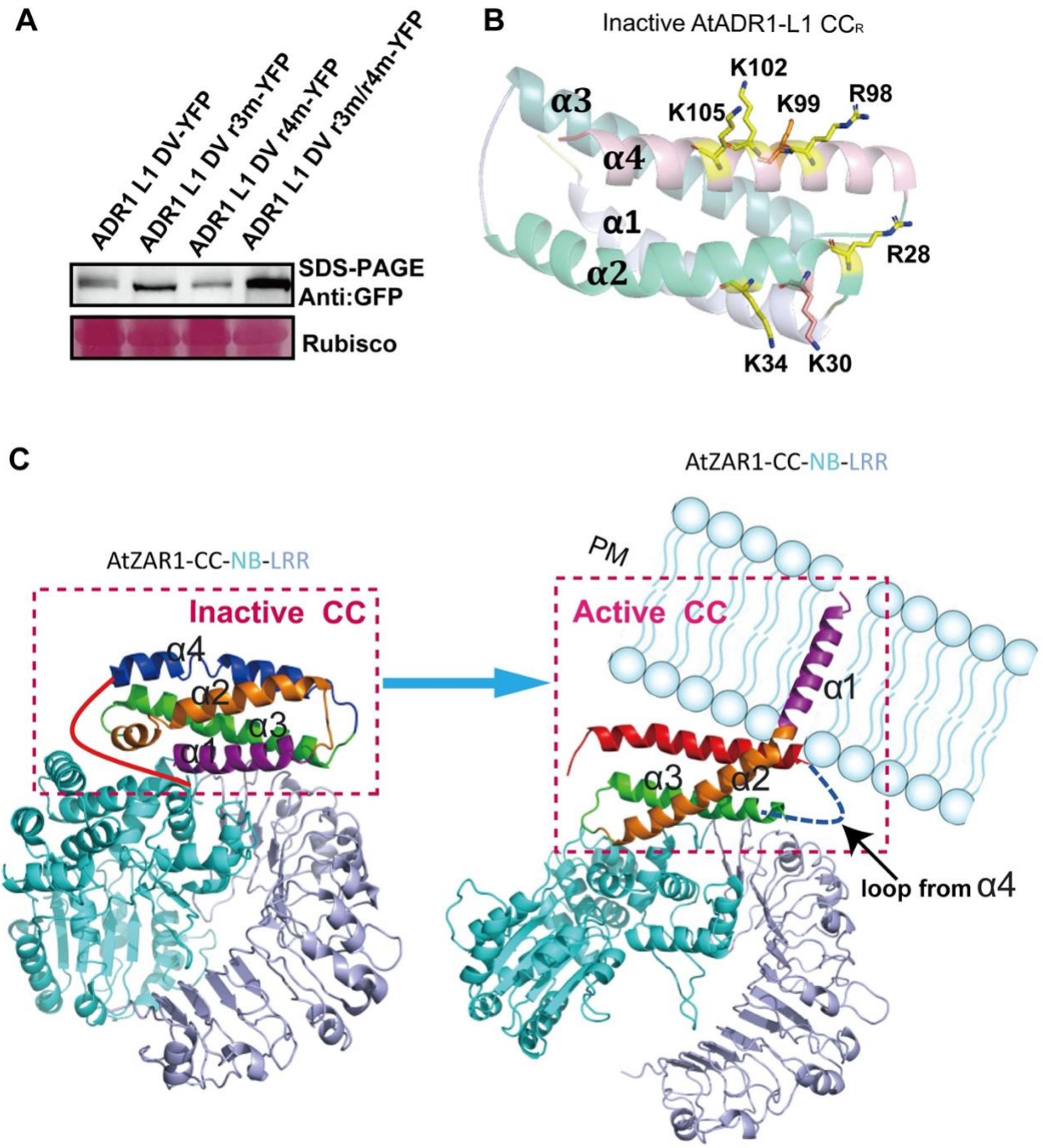

Figure S2 (A) Protein expression levels of AtADR1_L1 relevant mutants assayed by immunoblot. **(B)** Cartoon presentation of an AlphaFold AtADR1-L1 structure highlighting the positively charged residues involved in r3m and r4m. **(C)** Cartoon presentation of AtZAR1 in resting state (PDB: 6J5W) and in active state (PDB: 6J5T) highlighting the conformational changes in the CC domain and PM association.

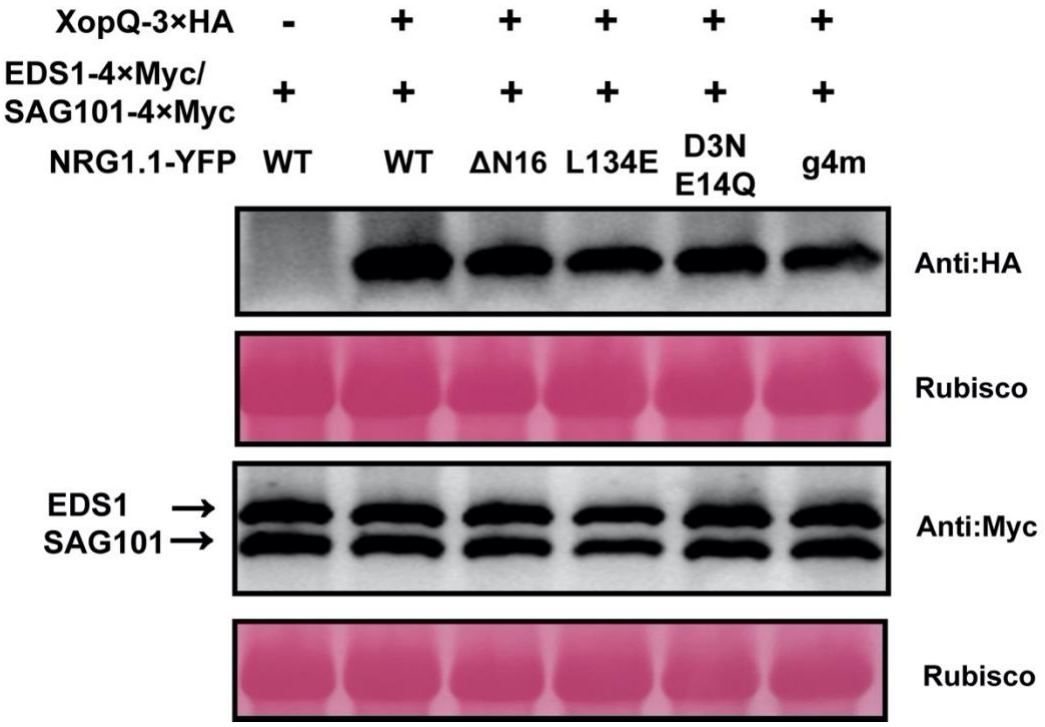

Figure S3 Protein levels of XopQ, EDS1 and SAG101 from experiments displayed in Figure 4A and 4B. HA-tagged XopQ and Myc-tagged EDS1/SAG101 were separated by SDS-PAGE and blotted for anti-HA and anti-Myc, respectively.

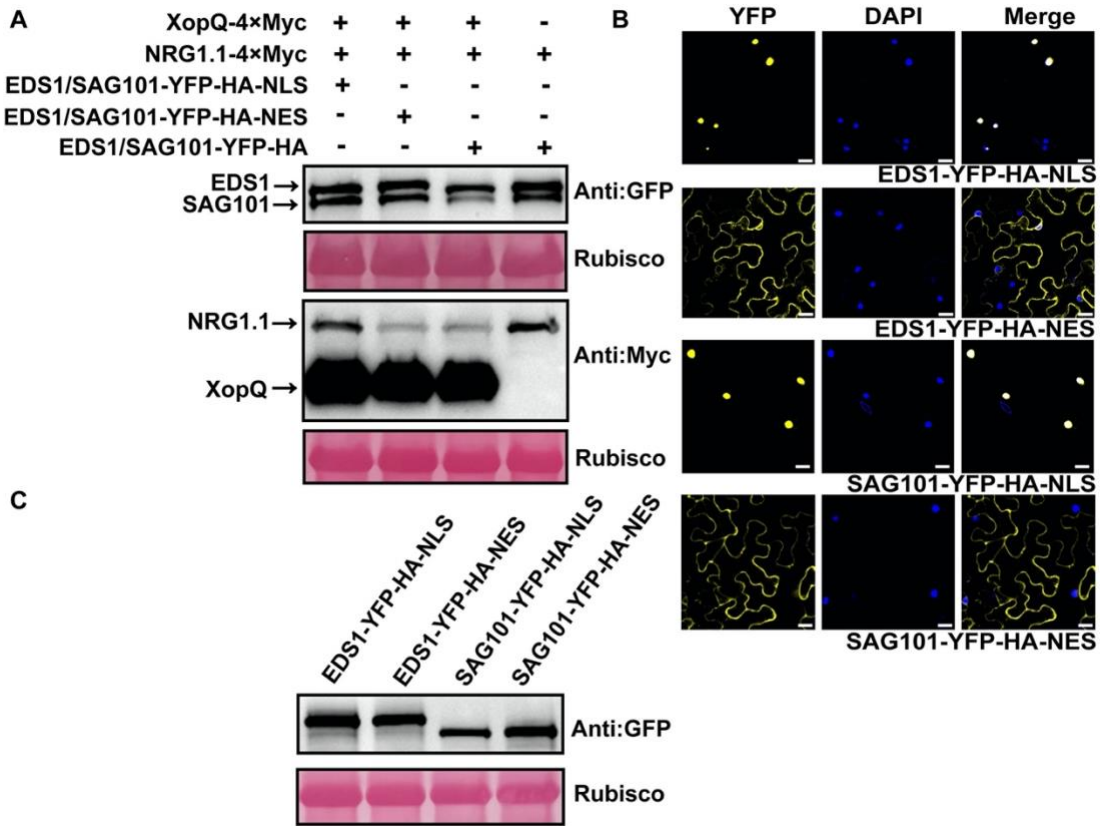

Figure S4 (A) Protein expression levels of samples from experiments displayed in Figure 4A. Total proteins were extracted from samples harvested at 26h post infiltration. Target proteins were separated by SDS-PAGE and blotted with the appropriate antibodies. **(B)** Confocal images showing the subcellular localization of EDS1-YFP-HA-NLS, EDS1-YFP-HA-NES, SAG101-YFP-HA-NLS and SAG101-YFP-HA-NES. Images were photographed at 48h post infiltration in *Nb* leaves. Nuclei were stained with DAPI (4', 6-diamidino-2-phenylindole). Bars, 20 μm. **(C)** Protein accumulation of samples in (B) detected with anti-GFP antibody.

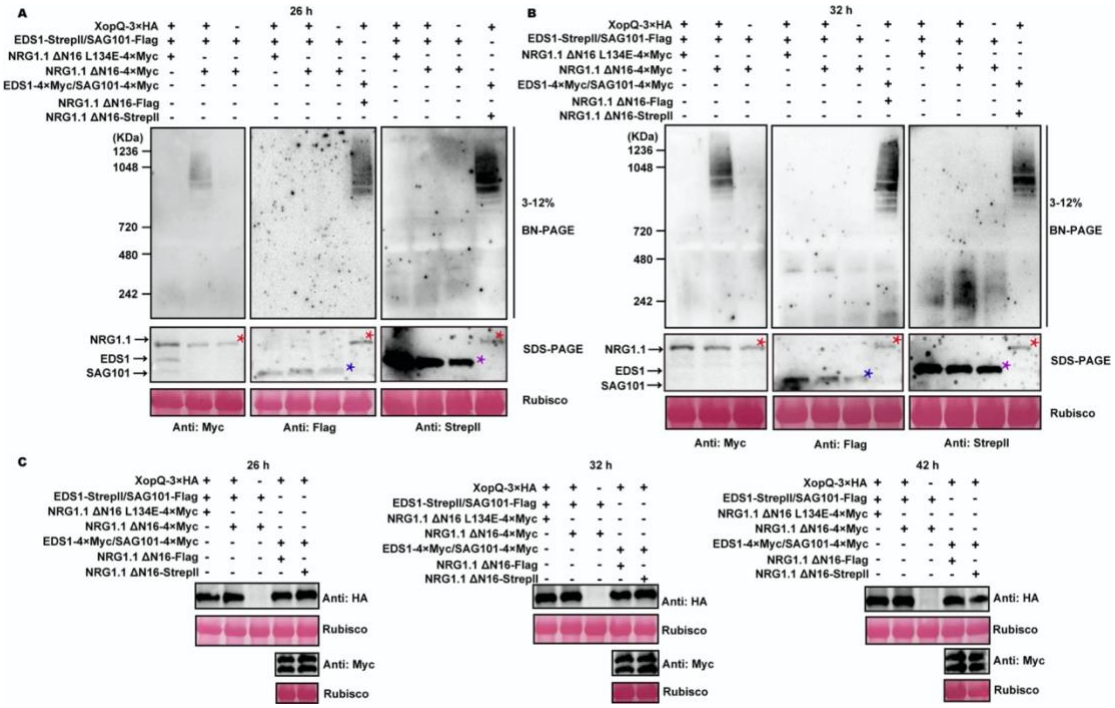

Figure S5 BN-PAGE assays showing that EDS1/SAG101 is not observed in an oligomeric complex with NRG1.1 at 26h **(A)** or 32h (**B)** after co-expression with XopQ in *Nb epss*. Red, purple and blue asterisks indicate NRG1.1, EDS1 and SAG101 bands, respectively. **(C)** Protein expression of XopQ, EDS1 and SAG101 as displayed in Figure 4B and Figure S5A and S5B was verified by SDS-PAGE. XopQ, EDS1/SAG101 were detected with anti-HA antibody and anti-Myc antibody, respectively.

Table S1 Gene ID of the 69 helper NLR homologs used in the alignment by CLustalW.

Gene	Gene ID (databases)[1]	Plant species
AtNRG1.1	At5g66900.1 (TAIR)	*Arabidopsis thaliana*
AtNRG1.2	At5g66910.1 (TAIR)	*Arabidopsis thaliana*
NbNRG1	NbS00018358g0013.1 (SGN)	*Nicotiana benthamiana*
AlNRG1	2614272850 (IMG)	*Arabidopsis lyrata*
AhNRG1	2614358615 (IMG)	*Arabidopsis halleri*
CrNRG1	2614531086 (IMG)	*Capsella rubella*
EhNRG1	2615507434 (IMG)	*Eutrema halophilum*
CsNRG1	2615787498 (IMG)	*Citrus sinensis*
CcNRG1	2614549921 (IMG)	*Citrus clementina*
PpNRG1	2615813723 (IMG)	*Prunus persica*
VvNRG1.1	649552880 (IMG)	*Vitis vinifera*
VvNRG1.2	649554972 (IMG)	*Vitis vinifera*
SpNRG1.1	2615336907(IMG)	*Salix purpurea*
SpNRG1.2	2615348770 (IMG)	*Salix purpurea*
RcNRG1	649572805 (IMG)	*Ricinus communis*
PtNRG1	2615290452 (IMG)	*Populus trichocarpa*
SlNRG1	Solyc02g090380.4.1 (SGN)	*Nicotiana benthamiana*
AtADR1	At1g33560.1 (TAIR)	*Arabidopsis thaliana*
AtADRL1 L1	At4g33300.1 (TAIR)	*Arabidopsis thaliana*
AtADRL1 L2	At5g04720.1 (TAIR)	*Arabidopsis thaliana*
NbADR1	Niben101Scf02422g02015.1 (SGN)	*Nicotiana benthamiana*
AlADR1	2614261905 (IMG)	*Arabidopsis lyrata*
AlADR1 L1	2614291476 (IMG)	*Arabidopsis lyrata*
AlADR1 L2	2614268259 (IMG)	*Arabidopsis lyrata*
AhADR1	2614369556 (IMG)	*Arabidopsis halleri*
CrADR1	2614512948 (IMG)	*Capsella rubella*
CrADR1 L1	2614509067 (IMG)	*Capsella rubella*
CrADR1 L2	2614505477 (IMG)	*Capsella rubella*
EhADR1	2615515499 (IMG)	*Eutrema halophilum*
EhADR1 L1	2615525947 (IMG)	*Eutrema halophilum*
EhADR1 L2	2615515499 (IMG)	*Eutrema halophilum*
GrADR1	2614796124 (IMG)	*Gossypium raimondii*
PtADR1	2615278681 (IMG)	*Populus trichocarpa*
CcADR1	2614532153 (IMG)	*Citrus clementina*
CsADR1	2615787425 (IMG)	*Citrus sinensis*
VvADR1	649539454 (IMG)	*Vitis vinifera*
SpADR1	2615316196 (IMG)	*Salix purpurea*
PpADR1	2615813687 (IMG)	*Prunus persica*
RcADR1	649560471 (IMG)	*Ricinus communis*
NbNRC2a	NbS00018282g0019.1 (SGN)	*Nicotiana benthamiana*
NbNRC2b	NbS00026706g0016.1 (SGN)	*Nicotiana benthamiana*
NbNRC3	NbS00011087g0003.1 (SGN)	*Nicotiana benthamiana*
NbNRC4a	NbS00002971g0007.1 (SGN)	*Nicotiana benthamiana*
NbNRC4b	NbS00016103g0004.1 (SGN)	*Nicotiana benthamiana*
NbNRCX	NbS00030243g0001.1 (SGN)	*Nicotiana benthamiana*
SlNRC1	Solyc01g090430.3.1 (SGN)	*Solanum lycopersicum*
SlNRC2	Solyc10g047320.2.1 (SGN)	*Solanum lycopersicum*
SlNRC3	Solyc05g009630.3.1 (SGN)	*Solanum lycopersicum*

Gene	Gene ID (databases)[1]	Plant species
SlNRC4a	Solyc04g007070.3.1 (SGN)	*Solanum lycopersicum*
SlNRC4b	Solyc04g007060.3.1 (SGN)	*Solanum lycopersicum*
SlNRC4c	Solyc04g007030.3.1 (SGN)	*Solanum lycopersicum*
SlNRCX	Solyc03g005660.4.1 (SGN)	*Solanum lycopersicum*
StNRC1a	PGSC0003DMT400066999 (SGN)	*Solanum tuberosum*
StNRC1b	PGSC0003DMT400066996 (SGN)	*Solanum tuberosum*
StNRC1c	PGSC0003DMT400066993 (SGN)	*Solanum tuberosum*
StNRC2a	PGSC0003DMT400080649 (SGN)	*Solanum tuberosum*
StNRC2b	PGSC0003DMT400080647 (SGN)	*Solanum tuberosum*
StNRC4a_1	PGSC0003DMT400041024 (SGN)	*Solanum tuberosum*
StNRC4a_2	PGSC0003DMT400069010 (SGN)	*Solanum tuberosum*
StNRC4a_3	PGSC0003DMT400069014 (SGN)	*Solanum tuberosum*
StNRC4a_4	PGSC0003DMT400041023 (SGN)	*Solanum tuberosum*
StNRC4b_1	PGSC0003DMT400019304 (SGN)	*Solanum tuberosum*
StNRC4b_2	PGSC0003DMT400019303 (SGN)	*Solanum tuberosum*
StNRC4b_3	PGSC0003DMT400019302 (SGN)	*Solanum tuberosum*
StNRC4b_4	PGSC0003DMT400019327 (SGN)	*Solanum tuberosum*
SmNRC1	SMEL4.1_12g003240.1 (SGN)	*Solanum melongena*
SmNRC3	SMEL4.1_10g001370.1 (SGN)	*Solanum melongena*
SmNRC4a	SMEL4.1_11g018090.1 (SGN)	*Solanum melongena*
SmNRC4b	SMEL4.1_11g018170.1 (SGN)	*Solanum melongena*

[1]TAIR, IMG and SGN are abbreviated from Arabidopsis Information Resource, Integrated Microbial Genomes and Solanaceae Genomics Network databases.

References

1. T. A. DeFalco, C. Zipfel, Review Molecular mechanisms of early plant pattern-triggered immune signaling. *Mol Cell* **81**, 3449-3467 (2021).
2. J. D. Jones, R. E. Vance, J. L. Dangl, Intracellular innate immune surveillance devices in plants and animals. *Science* **354** (2016).
3. P. Jacob *et al.*, Plant "helper" immune receptors are Ca2+-permeable nonselective cation channels. *Science* **373**, 420-+ (2021).
4. L. M. Jubic, S. Saile, O. J. Furzer, F. El Kasmi, J. L. Dangl, Help wanted: helper NLRs and plant immune responses. *Curr Opin Plant Biol* **50**, 82-94 (2019).
5. X. X. Liu, L. Wan, Molecular insights into the biochemical functions and signalling mechanisms of plant NLRs. *Molecular Plant Pathology* **23**, 772-780 (2022).
6. D. Lapin *et al.*, A Coevolved EDS1-SAG101-NRG1 Module Mediates Cell Death Signaling by TIR-Domain Immune Receptors. *Plant Cell* **31**, 2430-2455 (2019).
7. J. Gantner, J. Ordon, C. Kretschmer, R. Guerois, J. Stuttmann, An EDS1-SAG101 Complex Is Essential for TNL-Mediated Immunity in Nicotiana benthamiana. *Plant Cell* **31**, 2456-2474 (2019).
8. S. C. Saile *et al.*, Two unequally redundant "helper" immune receptor families mediate Arabidopsis thaliana intracellular "sensor" immune receptor functions. *Plos Biology* **18** (2020).
9. H. Adachi, L. Derevnina, S. Kamoun, NLR singletons, pairs, and networks: evolution, assembly, and regulation of the intracellular immunoreceptor circuitry of plants. *Current Opinion in Plant Biology* **50**, 121-131 (2019).
10. C. H. Wu *et al.*, NLR network mediates immunity to diverse plant pathogens. *Proc Natl Acad Sci U S A* **114**, 8113-8118 (2017).
11. J. Wang *et al.*, Ligand-triggered allosteric ADP release primes a plant NLR complex. *Science* **364** (2019).
12. G. Z. Bi *et al.*, The ZAR1 resistosome is a calcium-permeable channel triggering plant immune signaling. *Cell* **184**, 3528-+ (2021).
13. J. Wang *et al.*, Reconstitution and structure of a plant NLR resistosome conferring immunity. *Science* **364** (2019).
14. A. Forderer *et al.*, A wheat resistosome defines common principles of immune receptor channels. *Nature* **610**, 532-539 (2022).
15. Y. B. Zhao *et al.*, Pathogen effector AvrSr35 triggers Sr35 resistosome assembly via a direct recognition mechanism. *Sci Adv* **8**, eabq5108 (2022).
16. S. Horsefield *et al.*, NAD(+) cleavage activity by animal and plant TIR domains in cell death pathways. *Science* **365**, 793-799 (2019).
17. S. Ma *et al.*, Direct pathogen-induced assembly of an NLR immune receptor complex to form a holoenzyme. *Science* **370** (2020).
18. R. Martin *et al.*, Structure of the activated ROQ1 resistosome directly recognizing the pathogen effector XopQ. *Science* **370** (2020).
19. S. Huang *et al.*, Identification and receptor mechanism of TIR-catalyzed small molecules in plant immunity. *Science* **377**, eabq3297 (2022).

20. A. Jia *et al.*, TIR-catalyzed ADP-ribosylation reactions produce signaling molecules for plant immunity. *Science* **377**, eabq8180 (2022).
21. L. Wan *et al.*, TIR domains of plant immune receptors are NAD(+)-cleaving enzymes that promote cell death. *Science* **365**, 799-803 (2019).
22. K. Essuman, J. Milbrandt, J. L. Dangl, M. T. Nishimura, Shared TIR enzymatic functions regulate cell death and immunity across the tree of life. *Science* **377**, 486-+ (2022).
23. X. H. Sun *et al.*, Pathogen effector recognition-dependent association of NRG1 with EDS1 and SAG101 in TNL receptor immunity. *Nature Communications* **12** (2021).
24. Z. S. Wu, L. Tian, X. R. Liu, Y. L. Zhang, X. Li, TIR signal promotes interactions between lipase-like proteins and ADR1-L1 receptor and ADR1-L1 oligomerization. *Plant Physiology* **187**, 681-686 (2021).
25. Z. Gao, E. H. Chung, T. K. Eitas, J. L. Dangl, Plant intracellular innate immune receptor Resistance to Pseudomonas syringae pv. maculicola 1 (RPM1) is activated at, and functions on, the plasma membrane. *Proc Natl Acad Sci U S A* **108**, 7619-7624 (2011).
26. D. Qi, B. J. DeYoung, R. W. Innes, Structure-Function Analysis of the Coiled-Coil and Leucine-Rich Repeat Domains of the RPS5 Disease Resistance Protein. *Plant Physiology* **158**, 1819-1832 (2012).
27. Y. Belkhadir, Z. Nimchuk, D. A. Hubert, D. Mackey, J. L. Dangl, Arabidopsis RIN4 negatively regulates disease resistance mediated by RPS2 and RPM1 downstream or independent of the NDR1 signal modulator and is not required for the virulence functions of bacterial type III effectors AvrRpt2 or AvrRpm1. *Plant Cell* **16**, 2822-2835 (2004).
28. M. Hu, J. Qi, G. Bi, J. M. Zhou, Bacterial Effectors Induce Oligomerization of Immune Receptor ZAR1 In Vivo. *Mol Plant* **13**, 793-801 (2020).
29. S. C. Saile *et al.*, Arabidopsis ADR1 helper NLR immune receptors localize and function at the plasma membrane in a phospholipid dependent manner. *New Phytologist* **232**, 2440-2456 (2021).
30. C. Duggan *et al.*, Dynamic localization of a helper NLR at the plant-pathogen interface underpins pathogen recognition. *Proc Natl Acad Sci U S A* **118** (2021).
31. Z. S. Wu *et al.*, Differential regulation of TNL-mediated immune signaling by redundant helper CNLs. *New Phytologist* **222**, 938-953 (2019).
32. H. Adachi et al., An atypical NLR protein modulates the NRC immune receptor network. *bioRxiv* **doi: https://doi.org/10.1101/2021.11.15.468391** (2021).
33. A. Schultink, T. Qi, A. Lee, A. D. Steinbrenner, B. Staskawicz, Roq1 mediates recognition of the Xanthomonas and Pseudomonas effector proteins XopQ and HopQ1. *Plant J* **92**, 787-795 (2017).
34. S. Zhu *et al.*, SAG101 forms a ternary complex with EDS1 and PAD4 and is required for resistance signaling against turnip crinkle virus. *PLoS Pathog* **7**, e1002318 (2011).
35. B. J. Feys *et al.*, Arabidopsis SENESCENCE-ASSOCIATED GENE101 stabilizes and signals within an ENHANCED DISEASE SUSCEPTIBILITY1 complex in plant innate immunity. *Plant Cell* **17**, 2601-2613 (2005).
36. M. Bernoux *et al.*, Comparative Analysis of the Flax Immune Receptors L6 and L7 Suggests an Equilibrium-Based Switch Activation Model. *Plant Cell* **28**, 146-159 (2016).

37. V. Markovic, Y. Jaillais, Phosphatidylinositol 4-phosphate: a key determinant of plasma membrane identity and function in plants. *New Phytologist* **235**, 867-874 (2022).
38. Y. Dondelinger *et al.*, MLKL compromises plasma membrane integrity by binding to phosphatidylinositol phosphates. *Cell Rep* **7**, 971-981 (2014).
39. Q. Chai *et al.*, A bacterial phospholipid phosphatase inhibits host pyroptosis by hijacking ubiquitin. *Science* **378**, eabq0132 (2022).
40. Y. Zhong, Z. M. Cheng, A unique RPW8-encoding class of genes that originated in early land plants and evolved through domain fission, fusion, and duplication. *Sci Rep-Uk* **6** (2016).
41. D. C. Boyes, J. Nam, J. L. Dangl, The Arabidopsis thaliana RPM1 disease resistance gene product is a peripheral plasma membrane protein that is degraded coincident with the hypersensitive response. *P Natl Acad Sci USA* **95**, 15849-15854 (1998).
42. F. El Kasmi *et al.*, Signaling from the plasma-membrane localized plant immune receptor RPM1 requires self-association of the full-length protein. *P Natl Acad Sci USA* **114**, E7385-E7394 (2017).
43. B. P. M. Ngou, H. K. Ahn, P. T. Ding, J. D. G. Jones, Mutual potentiation of plant immunity by cell-surface and intracellular receptors. *Nature* 10.1038/s41586-021-03315-7 (2021).
44. M. H. Yuan *et al.*, Pattern-recognition receptors are required for NLR-mediated plant immunity. *Nature* 10.1038/s41586-021-03316-6 (2021).
45. R. N. Pruitt *et al.*, The EDS1-PAD4-ADR1 node mediates Arabidopsis pattern-triggered immunity. *Nature* **598**, 495-+ (2021).
46. Y. J. Li *et al.*, Plasma membrane-nucleo-cytoplasmic coordination of a receptor-like cytoplasmic kinase promotes EDS1-dependent plant immunity. *Nature Plants* **8**, 802-+ (2022).
47. H. N. Tian *et al.*, Activation of TIR signalling boosts pattern-triggered immunity. *Nature* **598**, 500-+ (2021).
48. J. Kourelis *et al.*, The helper NLR immune protein NRC3 mediates the hypersensitive cell death caused by the cell-surface receptor Cf-4. *PLoS Genet* **18**, e1010414 (2022).
49. M. P. Contreras *et al.*, Sensor NLR immune proteins activate oligomerization of their NRC helpers in response to plant pathogens. *EMBO J* 10.15252/embj.2022111519, e111519 (2022).
50. H. K. Ahn *et al.*, Effector-dependent activation and oligomerization of plant NRC class helper NLRs by sensor NLR immune receptors Rpi-amr3 and Rpi-amr1. *EMBO J* 10.15252/embj.2022111484, e111484 (2023).
51. J. M. Feehan et al., Oligomerisation of a plant helper NLR requires cell-surface and intracellular immune receptor activation. *bioRxiv* **doi:** https://doi.org/10.1101/2022.06.16.496440 (2022).
52. X. Liu *et al.*, RIN13-mediated disease resistance depends on the SNC1-EDS1/PAD4 signaling pathway in Arabidopsis. *J Exp Bot* **71**, 7393-7404 (2020).
53. G. E. Crooks, G. Hon, J. M. Chandonia, S. E. Brenner, WebLogo: a sequence logo generator. *Genome Res* **14**, 1188-1190 (2004).
54. F. W. Studier, Protein production by auto-induction in high density shaking cultures. *Protein Expr Purif* **41**, 207-234 (2005).